Heliyon 9 (2023) e16375

Contents lists available at ScienceDirect

Heliyon

journal homepage: www.cell.com/heliyon

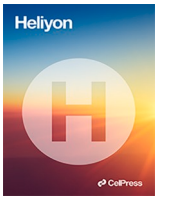

Research article

Calotropis gigantea stem bark extract activates HepG2 cell apoptosis through ROS and its effect on cytochrome P450

Pennapha Suknoppakit [a,1], Apirath Wangteeraprasert [b,1], Orakot Simanurak [a], Julintorn Somran [c], Supawadee Parhira [d,e,f], Dumrongsak Pekthong [e,f,g,*], Piyarat Srisawang [a,e,h,**]

[a] *Department of Physiology, Faculty of Medical Science, Naresuan University, Phitsanulok, 65000, Thailand*
[b] *Department of Medicine, Faculty of Medicine, Naresuan University, Phitsanulok 65000, Thailand*
[c] *Department of Pathology, Faculty of Medicine, Naresuan University, Phitsanulok, 65000, Thailand*
[d] *Department of Pharmaceutical Technology, Faculty of Pharmaceutical Sciences, Naresuan University, Phitsanulok, 65000, Thailand*
[e] *Center of Excellence for Innovation in Chemistry, Naresuan University, Phitsanulok 65000, Thailand*
[f] *Center of Excellence for Environmental Health and Toxicology, Faculty of Pharmaceutical Sciences, Naresuan University, Phitsanulok, 65000, Thailand*
[g] *Department of Pharmacy Practice, Faculty of Pharmaceutical Sciences, Naresuan University, Phitsanulok, 65000, Thailand*
[h] *Center of Excellence in Medical Biotechnology, Faculty of Medical Science, Naresuan University, Phitsanulok 65000, Thailand*

A R T I C L E I N F O

Keywords:
Calotropis gigantea
Hepatocellular carcinoma
Apoptosis
Reactive oxygen species (ROS)
CYP450

A B S T R A C T

The 95% ethanolic extract of the dry powder of *Calotropis gigantea* (*C. gigantea*) stem bark was separated by fractionation with different solutions to yield 4 fractions: dichloromethane (CGDCM), ethyl acetate (CGEtOAc), and water (CGW). This research focused on CGDCM-induced apoptosis in HepG2 cells with IC50 and above-IC50 values, which provide useful information for future anticancer applications. CGDCM had lower cytotoxicity on normal lung fibroblast IMR-90 cells than on HepG2 cells. Apoptotic induction of CGDCM was mediated by decreased fatty acid and ATP synthesis while increasing reactive oxygen species production. The effects of the four extracts on the activity of the four major CYP450 isoforms (CYP1A2, CYP2C9, CYP2E1 and CYP3A4) were determined using the CYP-specific model activity of each isoform. All four fractions of the extract were shown to be poor inhibitors of CYP1A2 and CYP2E1 (IC50 $>$ 1000 μg/mL) and moderate inhibitors of CYP3A4 (IC50 = 56.54–296.9 μg/mL). CGDCM and CGW exerted moderate inhibition activities on CYP2C9 (IC50 = 59.56 and 46.38 μg/mL, respectively), but CGEtOH and CGEtOAc exhibited strong inhibition activities (IC50 = 12.11 and 20.43 μg/mL, respectively). It is proposed that *C. gigantea* extracts at high doses have potential for further studies to develop alternative anticancer applications. Inhibiting CYP2C9 activity may also lead to drug-herb interactions.

* Corresponding author. Center of Excellence for Innovation in Chemistry, Naresuan University, Phitsanulok 65000, Thailand.
** Corresponding author. Department of Physiology, Faculty of Medical Science, Naresuan University, Phitsanulok, 65000, Thailand.
E-mail addresses: dumrongsakp@nu.ac.th (D. Pekthong), piyarats@nu.ac.th (P. Srisawang).
[1] These authors contributed equally to this work.

https://doi.org/10.1016/j.heliyon.2023.e16375
Received 9 February 2023; Received in revised form 24 April 2023; Accepted 15 May 2023
Available online 18 May 2023

1. Introduction

Hepatocellular carcinoma (HCC) is known to account for an aggressively high contribution of lethal associated cancers [1]. Although innovative chemotherapeutic studies have been undertaken as the primary treatment of cancer patients, their undesirable side effects and drug resistance still limit their efficiency. Several studies suggest that a plant extract applied as an alternative cancer treatment can reduce side effects and produce potent efficacy as a chemotherapeutic treatment [2,3].

Calotropis gigantea (*C. gigantea*) has been shown to treat various diseases, including cancer [4]. Flower extracts of *C. gigantea* inhibited the cell proliferation of mice bearing Ehrlich's ascites carcinoma [5]. The anti-proliferation of leaf extracts of *C. gigantea* against WiDr colon cancer cells had an IC50 of 48.5 μg/mL after 24 h of incubation [6]. The entire portion of *C. gigantea* extracts showed cytotoxic efficiency against lung cancer cells [7]. The root extracts of *C. gigantea* possess a higher level of effective anti-proliferation after treatment in breast cancer T47D cells than the leaf and flower extracts [8]. The extracts from the leaves and stems of *C. gigantea* triggered apoptosis in MCF-7 cells [9]. Several underlying pathways of the anticancer action of *C. gigantea* have been reported. Suppression of antioxidant expression and increased reactive oxygen species (ROS) production were reported in the stem bark extract from *C. gigantea*, including the dichloromethane fraction, against colon cancer cells [10], whole plant extracts [7], and the cardenolides coroglaucigenin, extracted from stems and leaves [11], after treating lung cancer cells. In addition, ROS production was increased and associated with apoptosis when cancer cells were treated with bioactive chemicals from other plant extracts that have compounds similar to those in *C. gigantea* extracts, such as flavonoids, triterpenoids, and phenolics [12–14].

Fatty acid levels have been shown to contribute to apoptotic cancer cell death. Several plant extracts that express anticancer activity inhibit the synthesis of fatty acids. Apoptosis was observed with decreased expression of the enzyme in the pathway of the synthesis of fatty acid, fatty acid synthase (FASN), after treatment with the diterpene kahweol, extracted from *Coffea arabica* beans [15]. In gallbladder carcinoma cells, α-mangostine induced apoptosis by inhibiting the expression of the lipogenesis enzymes FASN and acetyl-CoA carboxylase (ACC) [16]. Sulforaphane, a phytochemical found naturally as glucoraphanin (thioglucoside conjugate) in cruciferous vegetables, triggered apoptosis in LNCaP and 22Rv1 prostate cancer cells by inhibiting ACC1 and FASN expression for fatty acid synthesis [17]. Overall, inhibition of fatty acid production is considered one of the potential targets for the anticancer effects of plant extracts. Additionally, the mechanism underlying apoptosis induction by plant extracts demonstrated a correlation with a decrease in adenosine triphosphate (ATP) synthesis. Engeletin, a flavanonol glycoside, triggered apoptosis associated with inhibition of ATP synthesis in human lung cancer cells [12,18]. A decrease in ATP levels was suggested to involve the apoptotic effect of stem bark extracts of *C. gigantea*, the dichloromethane fraction, reported in human colorectal cancer cells [10].

Cytochrome (CYP) 450 is a group of CYP450 enzymes or isozymes on the cell wall of the endoplasmic reticulum that are important for phase I drug metabolism. Each CYP450 enzyme contains a different protein and heme (isozyme). Most drugs or herbal extracts are metabolized through the CYP450 system. For future applications in predicting drug-herb interactions, it is worthwhile to explore the effect of *C. gigantea* extracts on the CYP450 system, focusing on the four major isoforms (CYP1A2, CYP2C9, CYP2E1, and CYP3A4).

Consequently, our current study investigated the potential anticancer properties of stem bark extracts from *C. gigantea* on HepG2 cells at concentrations above the IC50. The cytotoxic effect of the extracts was evaluated on cancer cells, and the underlying mechanism involved the formation of ROS, fatty acids, and ATP levels. The interaction between *C. gigantea* extracts and CYPs 450 (isoforms CYP1A2, CYP2C9, CYP2E1, and CYP3A4) was also investigated. For applications as alternatives with increased anticancer treatment efficacy, this study provides basic knowledge for the ongoing investigation of potential targeted treatments from plant extracts and prospective drug-herb interactions.

2. Materials and methods

2.1. Plant material

The bark from the stem of *C. gigantea* was harvested from northern Thailand, Thoen District, Lampang Province, from 2015 to 2018. The collection of plants for research purposes in accordance with the national guidelines was approved with the permitted number 0278 under compliance with the Plant Varieties Protect Act B.E. 2542 (1999) Section 53 from the Department of Agriculture, Ministry of Agricultural and Cooperatives, Thailand. The *C. gigantea* herbarium specimen (voucher No. 005194) has been identified elsewhere [10]. The shed-dried stem bark was kept at 30 ± 5 °C room temperature for further sample preparation.

2.2. Sample preparation

After combining 3 kg of the shed-dried stem bark of *C. gigantea*, 95% ethanol (9 L × 3 times, AR grade, Thailand) was used for the extraction under 1 h of ultrasonic-assisted extraction at 30 ± 5 °C room temperature. The separation of ethanolic solution from plant residue was performed by filtration. To obtain ethanolic crude extract (CGEtOH), evaporation at 45 °C with a rotary evaporator (Buchi, Switzerland) was performed. By following the same protocol as our previous report [10], CGEtOH (100 g) was fractionated to yield 3 fractions: dichloromethane (CGDCM), ethyl acetate (CGEtOAc) and water (CGW). All solvents used for sample preparation were AR grade (Lab-scan, Thailand). Four tested extract fractions, CGEtOH, CGDCM, CGEtOAc, and CGW, were maintained at 4 ± 3 °C in the refrigerator.

2.3. Determination of selected phytochemical and cardenolide contents

The total cardiac glycoside, total triterpenoid and total phenolic contents of the tested samples were determined by colorimetric assay following the reported protocols [19–21]. In each fraction, the calactin and calotropin contents were measured using high-performance liquid chromatography (HPLC) reported in previous studies [10,22], which was slightly modified from the protocol described by Kharat and Kharat [9].

2.3.1. Total cardiac glycoside content

The method described by Tofighi et al. [21] was slightly modified and used to determine the total cardiac glycoside content of the samples. One milliliter of sample solution in 50% ethanol (1 mg/mL) was added to one mL of freshly prepared Baljet's reagent [1% picric acid (95 mL) mixed with 10% NaOH solution (5 mL)]. The reaction mixture was incubated at room temperature (30 ± 5 °C) in the dark for 1 h, diluted with 2 mL of purified water, and then the absorbance was measured at 495 nm using a UV/Vis spectrophotometer (Shimadzu UV-1800, Japan). The total cardiac glycoside content was calculated from a calibration curve of digoxin (Sigma–Aldrich, USA, 5–50 μg/mL, as following Eq. (1): $Y = 0.0153X+0.0502$, $R^2 = 0.9990$, where Y, X and R^2 represent the absorbance of digoxin at 495 nm, the concentration of digoxin (μg/mL) and the linear correlation coefficient, respectively). The total cardiac glycoside content was presented as milligrams of digoxin equivalents per gram of extract (mg DXE/g extract). The independent experiments were performed three times.

2.3.2. Total triterpenoid content

The total triterpenoid content was measured according to the method proposed by Chang et al. [20] with some modifications. In brief, 200 μL of 1 mg/mL sample solution in glacial acetic acid was mixed well with a 5% vanillin-acetic acid solution (1 mL) and 1.8 mL of sulfuric acid. The reaction mixture was then heated in a 70 °C water bath for 30 min before cooling to room temperature (30 ± 5 °C). In the last step, 2 mL glacial acetic acid was added and mixed well before determining its absorbance at 575 nm. The total triterpenoid content was calculated from a calibration curve (2–40 μg/mL) of ursolic acid (Tokyo Chemical, Japan) with the following Eq. (2): $Y = 0.0453X - 0.0943$, $R^2 = 0.9989$, where Y, X, and R^2 stand for the absorbance of ursolic acid at 575 nm, the concentration of ursolic acid (μg/mL), and the linear correlation coefficient, respectively. The total triterpenoid contents were reported as milligrams of ursolic acid equivalents per gram of extract (mg UAE/g extract).

2.3.3. Total phenolic content

The method described by Baba and Malik [19] with slight differences was used to determine the total phenolic content of the *C. gigantea* stem bark extracts. One milliliter of sample solution (1 mg/mL) was rigorously mixed with 1 mL of 1 : 10 Folin-Ciocalteu reagent (Merck, Germany) for 5 min, and then 1 mL of saturated sodium bicarbonate (60 g/L) was added. The reaction mixture was allowed to stand for 90 min in the dark at ambient temperature (30 ± 5 °C), and then the absorbance was measured at 725 nm using a UV/Vis spectrophotometer. A standard curve of gallic acid (Sigma-Aldrich, China. 7–13.3 μg/mL, as following Eq. (3): $Y = 0.1439X - 0.0684$, $R^2 = 0.9974$, Y, X and R^2 are the absorbance of gallic acid at 725 nm, the concentration of gallic acid (μg/mL) and the linear correlation coefficient, respectively) was used to calculate total phenolic contents of the samples and then expressed as milligram gallic acid equivalents per gram of extract (mg GAE/g extract).

2.3.4. Calotropin and calactin contents

The contents of calotropin and calactin in four tested samples were measured by using high-performance liquid chromatography (HPLC) with the same protocols as our previous studies [10,22], which were slightly modified from the method described by Kharat and Kharat [9]. Briefly, the test samples (5 mg/mL) were dissolved in methanol and then injected (20 μL) into the HPLC system (Shimadzu pump LC-10ATvp, Japan) by using an ultraviolet/visible detector at 222 nm. Phenomenex Luna® C18(2) (3 μm, 150 mm × 4.6 mm) was used as the stationary phase. The isocratic mobile phase [55% aqueous methanol (HPLC grade, LabScan, Thailand)] was used to elute the samples at a flow rate of 1 mL/min for 15 min. The standard calotropin and calactin used in this study were identified elsewhere [10,22,23]. The contents of calotropin and calactin (mg/10 g extract) in each sample were calculated from the calotropin and calactin standard curves [0.2–10 μg/mL; as following Eq. (4): $Y_1 = 23512X_1 - 1483$, $R^2 = 0.9972$ for calotropin and Eq. (5): $Y_2 = 35279X_2 - 4775$, $R^2 = 0.9949$ for calactin, where Y_1 = peak area at a retention time of approximately 7.5 ± 0.13 min, Y_2 = peak area at a retention time of approximately 11.5 ± 0.23 min, X_1 = concentration of calotropin (μg/mL) and X_2 = concentration of calactin (μg/mL)]. The experiments were performed in triplicate.

2.4. Cell culture

Human HCC, HepG2 cells (JCRB1054) (JCRB Cell Bank, Japan) and normal lung fibroblast IMR-90 cells (JCRB9054) (JCRB Cell Bank, Japan) were grown in Dulbecco's modified Eagle's medium (DMEM) (Corning, USA) supplemented with 10–15% fetal bovine serum (Gibco, USA) to obtain complete growth medium. Incubation conditions for cells were 37 °C with 5% CO_2 in the incubator.

2.5. Anti-proliferative effect detection by MTT

The cytotoxic influence of the extracts after treatment for 24 h was examined with the cellular reaction of MTT: 3-(4,5-dimethylthiazol-2-yl)-2,5-diphenyl-2H-tetrazolium bromide (Merck, Germany), with a 37 °C incubation in 4 h. In living cells, yellow MTT

dyes are converted to a DMSO-soluble purple formazan crystal by the mitochondrial reductase enzyme, followed by detection with a 595 nm optical density (OD) microplate reader (Synergy, BioTek, USA). Data were calculated using GraphPad Prism9 software.

2.6. Cell viability detection by crystal violet assay

Cell viability was examined using crystal violet (Sigma, USA). After treatment for 24 h, 0.25% crystal violet in 70% ethanol was used to incubate cells at room temperature for 30 min [24]. Crystal violet triarylmethane dye binds to ribose-type DNA molecules in viable cells. The purple formazan crystals were examined using an inverted optical microscope (IX71, Olympus, Japan).

2.7. Wound healing assay

After incubation for 48 h in a 12-well plate (Corning, USA), HepG2 cells reached 80% cell monolayer density. Then, a scraping procedure was performed to produce a gap between cells in each well. After treatment with the extract, the gap distance was monitored under an inverted optical microscope at 4X magnification and calculated using OLYMPUS cellSens Standard software.

2.8. Detection of apoptosis by Hoechst 33342 staining

After 24 h of treatment, HepG2 cells seeded on a cover slip in a 35 mm culture dish were collected, fixed with 4% formaldehyde, and stained with Hoechst 33342 dye. Fluorescence microscopy was applied to determine the stained cells (BX53F2, Olympus, Japan).

2.9. Mitochondrial membrane potential (MMP) dissipation determination using JC-1 staining

After HepG2 cells were treated for 24 h, cells seeded on a coverslip in a 35-mm culture dish were collected, fixed with 4% formaldehyde, and stained with a Mitochondrial Membrane Potential Probe (JC-1 dye, Invitrogen, USA). A cell exhibiting red fluorescence as aggregation of JC-1 in mitochondria represents healthy MMP, while green fluorescence as the cytosolic monomeric form represents depolarization of MMP. After staining, the cells were visualized using fluorescence microscopy.

2.10. Flow cytometry analysis of apoptosis

To detect the stage of apoptosis after 24 h of treatment in HepG2 cells, the double-stained dyes annexin V/Alexa Fluor 488 conjugate (A13204, Invitrogen, USA) and propidium iodide (PI) (P3566, Invitrogen, USA) were applied to stain cells. The apoptotic cells were analyzed with a CytoFLEX flow cytometer and CytExpert version 2.4.0.28 software (Beckman Coulter, USA).

2.11. Analysis of MMP using flow cytometry

Following an overnight treatment of HepG2 cells, cells were collected for incubation with 5,5′,6,6′-tetrachloro-1,1′,3,3′-tetraethylbenzimidazolylcarbocyanine iodide (JC-1; CBIC2(3)) (Invitrogen, USA) to detect MMP. The data were analyzed and measured by CytoFLEX flow cytometry with CytExpert software.

2.12. Detection of cleaved caspase-3 expression with fluorescence staining

Following a 24-h treatment, HepG2 cells seeded on a coverslip were collected and fixed with 4% formaldehyde. Cells were then incubated with the primary antibody anti-cleaved caspase-3 (D175; Cell Signaling Technology, USA) and the secondary antibody goat anti-rabbit IgG H&L (Alexa Fluor® 488) (ab150077, Abcam, USA). Hoechst 33342 dye was used to stain nuclei. Fluorescence microscopy was used to visualize the stained cells.

2.13. Detection of intracellular ROS by fluorescence H2DCFDA staining

After HepG2 cells were treated for 24 h, cells seeded on a coverslip in culture dishes were fixed with 4% formaldehyde and stained with the ROS detection fluorescent dye H2DCFDA (2′,7′-dichlorodihydrofluorescein diacetate) (D399, Thermo Fisher Scientific, USA) to detect intracellular ROS. Hoechst 33342 dye was used as a nuclear counterstain. Fluorescence microscopy was used to visualize the stained cells.

2.14. Determination of intracellular ROS levels

After HepG2 cells were treated for 24 h, the H2DCFDA-Cellular ROS Assay Kit (ab113851: Abcam, USA) was applied to measure intracellular ROS levels following the instructions of the manufacturer. The fluorescence intensity was measured and analyzed by a microplate reader (SpectraMax iD3, Molecular Devices, USA) at an excitation wavelength of 485 nm and an emission wavelength of 535 nm.

2.15. Determination of intracellular ROS with flow cytometry

Following a 24-h treatment, the fluorescent dye H2DCFDA (2′,7′-dichlorodihydrofluorescein diacetate) (D399, Thermo Fisher Scientific, USA) was applied to detect intracellular ROS levels. The cells permeable to H2DCFDA were oxidized to the 2′,7′-dichlorofluorescein (DCF) fluorescent form, which was then measured by CytoFLEX flow cytometry and analyzed by CytExpert software.

2.16. Determination of intracellular fatty acid levels

After 24 h of treatment in HepG2 cells, the intracellular fatty acid levels were measured and analyzed using a Nonesterified Free Fatty Acids (NEFA) Colorimetric Assay Kit (E-BC-K013-M, Elabscience, USA) following the instructions of the manufacturer. The optical density at 715 nm was measured using a microplate reader. Data were calculated using GraphPad Prism9 software.

2.17. Determination of intracellular ATP level

After 24 h of treatment in HepG2 cells, the luminescent ATP Detection Assay kit (ab113849: Abcam, USA) was applied to measure the levels of intracellular ATP following the instructions of the manufacturer. Using ATP and O_2, luciferase oxidizes luciferin to produce oxyluciferin, which was detected using a microplate reader (SpectraMax iD3, Molecular Devices, USA).

2.18. Determination of protein expression by western blotting

After HepG2 cells were treated for 24 h, intracellular proteins were collected from lysate cells by adding a cocktail of proteinase inhibitor (HIMEDIA, India) in the Mammalian Protein Extraction Reagent (M-PER) (Thermo Fisher Scientific, USA) followed by using a bicinchoninic acid assay reagent (Thermo Fisher Scientific, USA) to detect protein concentration. An equal quantity of each sample protein was applied to SDS–PAGE: sodium dodecyl sulfate–polyacrylamide gel electrophoresis. Proteins were transferred to PVDF membranes (Bio-Rad, USA), and nonspecific blocking was then performed. Next, the membranes were incubated overnight at 4 °C with primary antibodies, including rabbit polyclonal β-cell lymphoma 2 (Bcl-2) (PA1-30411, Thermo Fisher Scientific, USA), rabbit polyclonal SOD2/MnSOD (AF5144, Affinity bioscience, USA), rabbit polyclonal catalase (DF7545, Affinity bioscience, USA), and mouse monoclonal β-actin (8H10D10, Cell Signaling Technology, USA). Then, secondary antibodies were applied to the membrane at 4 °C for 4 h, including horseradish peroxidase-conjugated goat anti-rabbit (65–6120, Invitrogen, USA) or anti-mouse (A28177, Invitrogen, USA) antibodies. To detect protein bands, the membrane was then incubated with Luminata Forte Western horseradish peroxidase (HRP) substrate (Merck Millipore, USA). Then, detection of protein bands was performed with chemiluminescence (Image Quant LAS 4000; GE Healthcare Life Sciences, USA), and the percentages of protein expression are presented as relative protein/β-actin levels. ImageJ version 1.46 was used to calculate the data.

2.19. Determination of CYPs 450 activity (isoform 1A2, 2C9, 2E1 and 3A4)

CYP450 activity (isoform 1A2, 2C9, 2E1 and 3A4) was determined in pooled human liver microsomes (KaLy Cell Company, France) by incubating the four extract fractions, CGEtOH, CGDCM, CGEtOAc and CGW, of *C. gigantea* with specific substrates and then measuring by using the appropriate detectors as described below.

2.19.1. CYP1A2-dependent ethoxyresorufin-O-de-ethylase assay

The method used to measure CYP1A2 activity followed the protocols reported in a previous study [25]. Briefly, incubation of 0.02 mg protein of human liver microsomes, the substrate, 7-ethoxyresorufin (6.5 μM in Tris buffer pH 7.4), and 2 μL of tested extracts (0.1–1000 μg/mL) or DMSO (negative control) or α-naphthoflavone (positive control) in a final volume of 100 μL was applied at 37 °C. Initially, NADPH (10 mM, 20 μL, Sigma–Aldrich, Singapore) was added to activate the reaction, and then $ZnSO_4$ (87 mM, 15 μL) and $Ba(OH)_2$ (79 mM, 15 μL) were added to terminate the reaction. The precipitated protein was removed by centrifugation (4000 rpm, 5 min), and then 100 μL of the collected supernatant was mixed with 100 μL of glycine buffer pH 8.5. Detection of resorufin, a fluorescent metabolite, was performed at excitation/emission wavelengths of 530 nm/580 nm. Data are presented in pmol of resorufin formed/min/mg microsomal proteins.

2.19.2. Analysis of CYP2C9-dependent tolbutamide hydroxylase

A method conducted by Relling et al. was used in this study to determine CYP2C9 activity via tolbutamide hydroxylation. The first step was incubation of human liver microsomes (0.02 mg protein) and tolbutamide (250 mM in Tris buffer pH 7.4 supplemented with $MgCl_2$ and EDTA) with a total volume of 200 μL. *C. gigantea* extracts (0.1–1000 μg/mL), DMSO (negative control) or sulfaphenazone (positive control) (2 μL) were added to the mixture. NADPH (10 mM, 25 μL) was added to start the reaction and then incubated at 37 °C for 45 min, followed by adding ice-cold acetonitrile (125 μL) before being centrifuged at 4000 rpm for 5 min for termination of the reaction. HPLC-UV spectrophotometric analysis at 230 nm was used to analyze the supernatant. The internal standard curve of 4-hydroxytolbutamide was used for quantification. The data were demonstrated in pmol 4-hydroxytolbutamide formed/min/mg microsomal proteins [26].

2.19.3. Analysis of CYP2E1-dependent p-nitrophenol hydroxylation

The analysis of paranitrophenol hydroxylation was performed by following a method previously described by Allis and Robinson et al. Briefly, 0.25 mg protein of human liver microsomes was added and mixed with *p*-nitrophenol (500 μM in Tris buffer, pH 7.4) and 2 μL of tested extracts (0.1–1000 μg/mL), DMSO (negative control) or disulfuram (positive control) in a final volume of 100 μL. Starting the reaction, NADPH (1 mM, 20 μL) was added to the solution and then incubated at 37 °C for 30 min. Then, 50% trichloroacetic acid (20 μL) was added to stop the reaction, followed by centrifugation at 4000 rpm for 5 min. Then, 100 μL of the collected supernatant was mixed with NaOH solution (10 M, 20 μL). HPLC-UV at 535 nm was used for detection. Data are presented as pmol 4-nitrocatheol formed/min/mg microsomal proteins [27].

2.19.4. CYP3A4-dependent testosterone hydroxylase assay

The method used for measurement of testosterone 6β-hydroxylation followed the previous study conducted by Pearce et al. In brief, human liver microsomes (0.20 mg protein) were mixed with testosterone (250 μM in phosphate buffer pH 7.4 supplemented with $MgCl_2$ and EDTA, 200 μL) followed by adding 2 μL of four tested extracts (0.1–1000 μg/mL), DMSO (negative control) or ketoconazole (positive control). Starting the reaction, NADPH (1 mM, 20 μL) was added to the solution, followed by incubation for 8 min at 37 °C. To terminate the reaction, ice-cold acetonitrile (125 μL) was added to the solution, followed by centrifugation at 12,000 rpm for 5 min. Analysis of the collected supernatant was performed using HPLC-UV spectrophotometry at 230 nm. The internal standard curve of 11β-hydrooxytestosterone was used for quantification. Data were demonstrated in pmol 6β-hydroxytestosterone formed/min/mg microsomal proteins [28].

2.19.5. IC50 determinations

Initially, ethoxyresorufin concentration at 1 μM, tolbutamide (50 μM), *p*-nitrophenol (100 μM) and testosterone (100 μM) were selected to determine the effect of the *C. gigantea* extracts on the high capacity or low affinity components with *C. gigantea* extracts final concentrations in the incubation mixture were (0.1, 1, 10, 100, 500, 1000 μg/mL) of metabolism for each substrate. The selective CYP1A2, CYP2C9, CYP2E1 and CYP3A4 activity inhibitors were α-naphthoflavone, sulfaphenazole, disulfiram, and ketoconazole, respectively. The IC50 values of *C. gigantea* extracts were determined using the logarithm plot of inhibitor concentrations relative to the level of remaining activity with nonlinear regression analysis using GraphPad Prism 9 (GraphPad Co., Ltd., USA).

2.20. Statistical analysis

The data are presented as the mean ± SD. The significantly different data between the treatment and the control vehicle groups at $p < 0.05$ were analyzed using one-way analysis of variance (ANOVA) with Tukey's post hoc test analysis with Graph Prism Software version 9.

3. Results

3.1. Plant extraction, selected phytochemicals and cardenolide contents in the stem bark extracts from C. gigantea

The ultrasonic-assisted extraction of 3 kg shed dry stem bark of *C. gigantea* with 95% ethanol provided CGEtOH (152.0 g, 5.1% yield of dry plant). The liquid partition of 100 g of CGEtOH resulted in obtaining CGDCM (21.2 g, 21.2% yield of crude extract), CGEtOAc (0.7 g, 0.7% yield of crude extract) and CGW (57.3 g, 57.3% yield of crude extract).

Four extract fractions composed of CGEtOH, CGDCM, CGEtOAc and CGW were used for further determination of selected phytochemical contents, including total cardiac glycosides (36.4–178.2 mg DXE/g extract), triterpenoids (33.9–622.9 mg UAE/g extract) and phenolic compounds (4.5–29.7 mg GAE/g extract) (Table 1). The selected cardenolide levels in the extracts of *C. gigantea* stem bark ranged from 0.4 to 7.1 mg calotropin/10 g extract and 3.3–12.4 mg calactin/10 g extract. The results revealed that among the 4 extracts, CGDCM contained the highest levels of calactin (12.4 ± 0.46 mg/10 g extract) and total triterpenoids (622.9 ± 26.17 mg UAE/g extract), which were significantly higher than those of the other fractions, as well as high levels of other phytochemicals, both cardiac glycosides and phenolic compounds, and calotropin. CGEtOAc appeared to have the highest contents of total cardiac glycosides (178.2 ± 3.48 mg DXE/g extract) and total phenolic compounds (29.7 ± 0.57 mg GAE/g extract). The highest amount of

Table 1
The contents of selected phytochemicals, calotropin and calactin in the stem bark extracts of *C. gigantea*.

Extracts	Total cardiac glycoside (mg DXE/g extract)	Total triterpenoid (mg UAE/g extract)	Total phenolic (mg GAE/g extract)	Calotropin (mg/10 g extract)	Calactin (mg/10 g extract)
CGEtOH	75.9 ± 3.15	55.2 ± 10.72	15.9 ± 0.30	7.1 ± 1.24	8.0 ± 0.03
CGDCM	90.5 ± 7.41	622.9 ± 26.17	19.3 ± 0.75	3.9 ± 0.32	12.4 ± 0.46
CGEtOAc	178.2 ± 3.48	98.6 ± 7.51	29.7 ± 0.57	0.4 ± 0.04	3.3 ± 0.13
CGW	36.4 ± 2.43	33.9 ± 2.92	4.5 ± 0.20	6.5 ± 0.38	6.3 ± 0.58

Note: CGEtOH, CGDCM, CGEtOAc and CGW were the crude extract and four extract fractions: dichloromethane, ethyl acetate extract fraction and water extract fraction of *C. gigantea* stem bark, respectively. DXE, UAE and GAE are the digoxin equivalent, ursolic acid equivalent and gallic acid equivalent, respectively.

calotropin was in CGEtOH (7.1 ± 1.24 mg calotropin/10 g extract), followed by CGW and CGDCM, and the lowest amount was in CGEtOAc.

3.2. The cytotoxicity of the stem bark extract fractions from C. gigantea on HepG2 cells

Following the treatment of HepG2 cells for 24 h with various concentrations of four extract fractions, CGEtOH, CGDCM, CGEtOAc, and CGW, the IC50 values were CGEtOH>1500 μg/mL, CGDCM 219.25 ± 62.99 μg/mL, CGEtOAc 806.23 ± 355.67 μg/mL, and CGW>3000 μg/mL, respectively (Fig. 1A). The CGDCM fraction showing the highest effect on the antiproliferation of cells was chosen for subsequent experiments. In addition, sorafenib with an IC50 value of approximately 8 μM (data not shown) was applied as a positive control. The crystal violet test verified that the CGDCM fraction induced dose-dependent cytotoxicity in HepG2 cells relative to the control group (Fig. 1B). As shown in Fig. 1C and D of the wound healing assay, the vehicle control showed a reduction in the gap distance, while the gap distance remained wide following CGDCM treatment in HepG2 cells within 72 h. Our findings suggest that

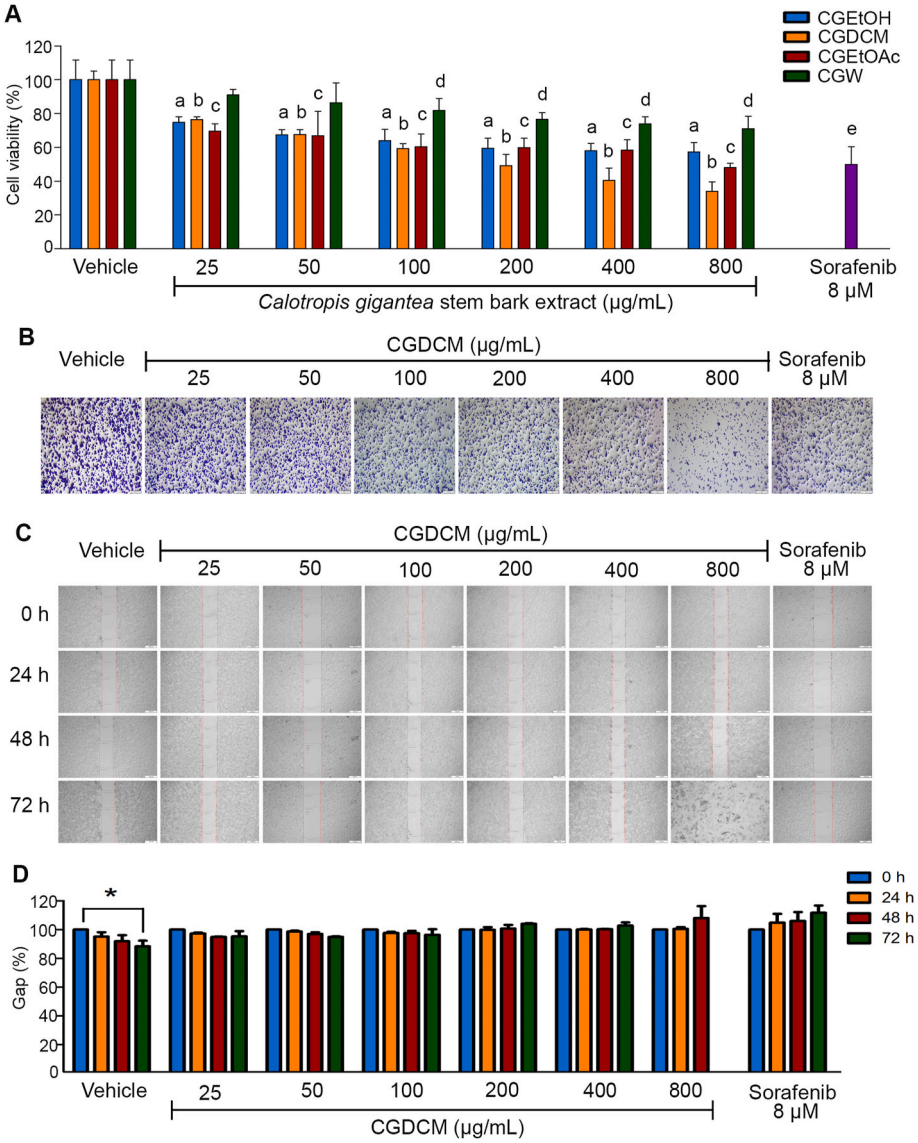

Fig. 1. The extracts from the stem bark of *C. gigantea* inhibit the viability of HepG2 cells. (A) HepG2 cells were treated for 24 h with various concentrations of four *C. gigantea* fractions, sorafenib, and a vehicle control consisting of 0.8% DMSO, as determined by the MTT assay. CGDCM was used to determine (B) the crystal violet assay, (C) migration assay, and (D) the percentage of calculated gap distance. Bars = 500 μm. Data are presented as the mean ± SD from at least three replicates, n = 3, and statistics were analyzed using one-way ANOVA with Tukey's HSD test. a, b, c, and d; $p < 0.05$ versus vehicle control treated with CGEtOH, CGDCM, CGEtOAc, and CGW, respectively. (For interpretation of the references to color in this figure legend, the reader is referred to the Web version of this article.)

CGDCM produces an antiproliferative effect on cell proliferation and suppresses the migration of HepG2 cells, similar to the effect of sorafenib.

3.3. Induction of apoptosis following CGDCM treatment in HepG2 cells involved a reduction in MMP

Hoechst 33342 and JC-1 staining were used to examine DNA fragmentation and the reduction in MMP in the apoptosis induction effect of CGDCM on HepG2 cells (Fig. 2). The CGDCM treatment produced apoptosis with increasing DNA fragmentation and decreasing MMP, which was similar to that found in sorafenib at 8 μM.

Based on the data from the MTT experiment, the CGDCM fraction with an IC50 of 200 μg/mL and higher than IC50 concentrations at 400 and 800 μg/mL were used to examine their cytotoxic effect on HepG2 cells at high dosages for basic knowledge to be applied in future anticancer therapeutic regimens.

As revealed in Fig. 3A and B, concentrations of 200 μg/mL, 400 μg/mL, and 800 μg/mL of CGDCM significantly triggered apoptosis in HepG2 cells relative to cells in the control vehicle. CGDCM at 800 μg/mL significantly increased apoptosis in comparison to CGDCM at 200 and 400 μg/mL. The apoptotic activity was demonstrated by the decrease in Bcl-2 protein expression (Fig. 3C and D, and Supplementary Fig. S1) and the increase in cleaved caspase-3 expression (Fig. 3E) with CGDCM concentration at 800 μg/mL, which was the most evident. In addition, the cytotoxic effect of CGDCM at concentrations of 200, 400, and 800 μg/mL showed less effect on IMR-90 cells than on HepG2 cells (Fig. 3F), indicating that CGDCM may be relatively safe for specific administration in anticancer therapy.

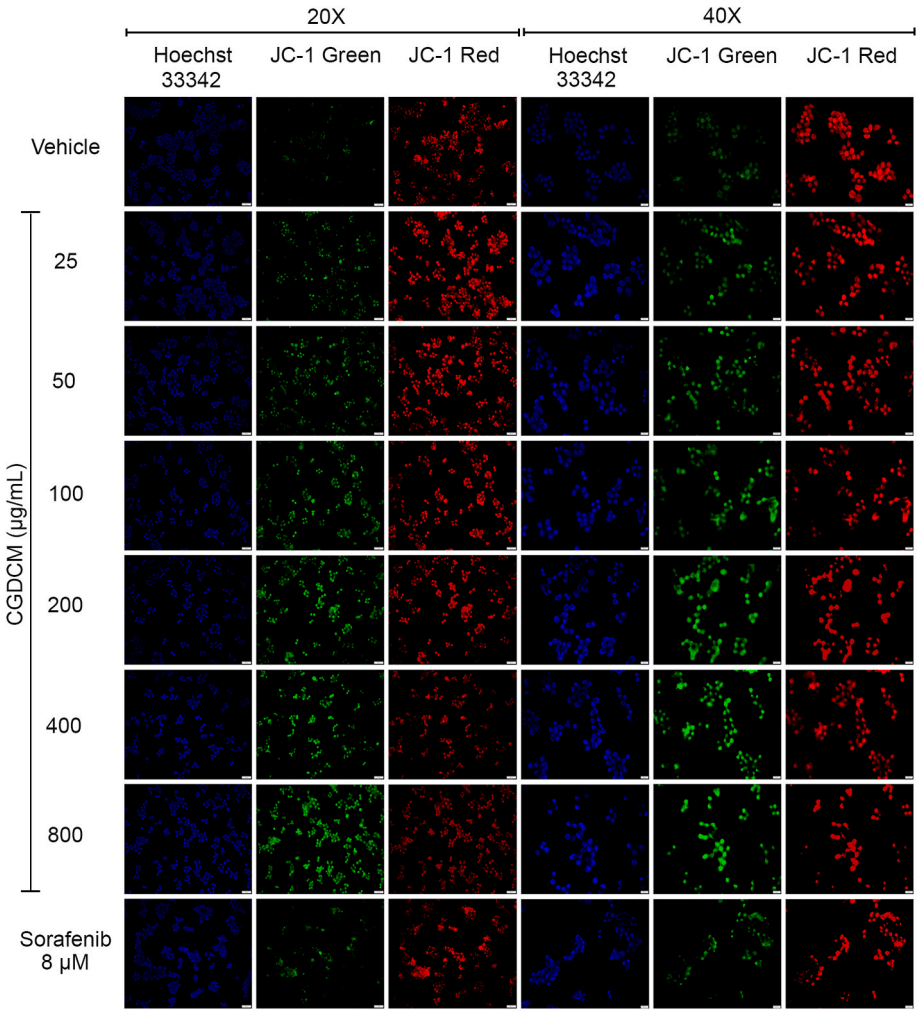

Fig. 2. Morphology of apoptotic cells was determined after 24 h of treatment with CGDCM, sorafenib at 8 μM, and vehicle control with 0.8% DMSO in HepG2 cells. Fluorescence microscopy was applied using Hoechst 33342 and JC-1 staining to visualize the fluorescence intensity, with bars = 500 μm.

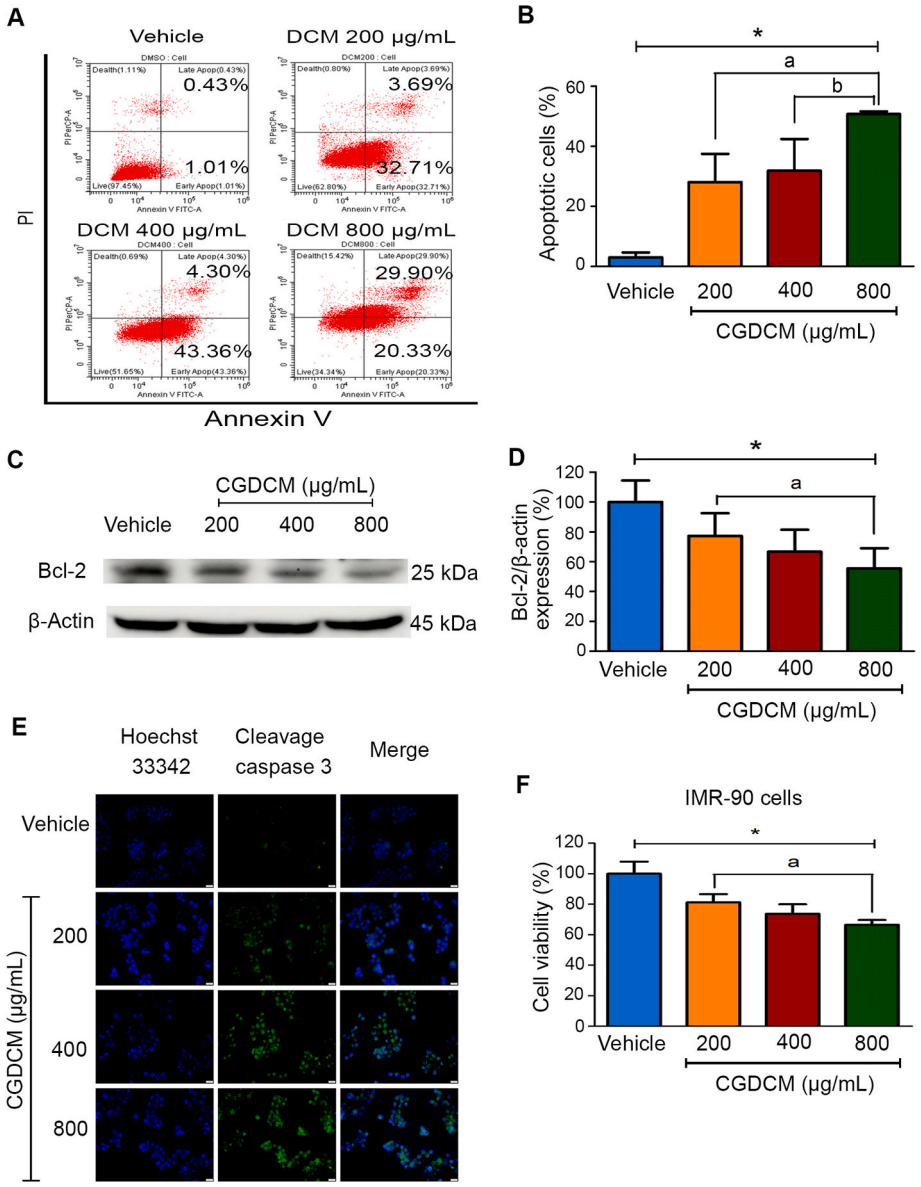

Fig. 3. Apoptotic induction in HepG2 cells treated with CGDCM at 200, 400, and 800 μg/mL and 0.8% DMSO as the vehicle control for 24 h. (A) Flow cytometry detection of apoptosis using double staining with annexin-V and PI. (B) The percentage of apoptotic cells is presented in the histogram. (C) Western blot image of the expression of Bcl-2 and (D) the relative expression level of Bcl-2/β-actin. The original uncropped western blots of Bcl-2 and β-actin are presented in the Supplementary Fig. S1. (E) The expression of cleaved caspase-3 was measured by immunofluorescence with Hoechst 33342-stained nuclei. (F) MTT analysis of IMR-90 cell viability after CGDCM treatment. Data are presented as the mean ± SD from at least three replicates, n = 3, and statistics were analyzed using one-way ANOVA with Tukey's HSD test. *p < 0.05 relative to the vehicle.

3.4. The mechanisms of apoptotic induction by CGDCM treatment in HepG2 cells involve suppression of fatty acid and ATP synthesis and activation of ROS production

De novo lipogenesis (DNL) is one of the potential targets of cancer therapeutic approaches [29,30]. Additionally, ATP and ROS generation are considered to be mechanisms involved in the apoptosis of colon cancer cells following treatment with *C. gigantea* stem bark extract [10]. Fig. 4A and B shows that suppressing fatty acid and ATP levels was involved in the induction of apoptosis of CGDCM at 200, 400, and 800 μg/mL. As shown in Fig. 4C and D, increased ROS production was associated with cancer cell apoptosis, consistent with previous studies [7,31]. In addition, following CGDCM treatment, the expression of the antioxidant enzymes SOD2 and catalase decreased (Fig. 4E–G and Supplementary Fig. S2), suggesting an increase in oxidative damage by ROS-induced apoptotic cell death in HepG2 cells.

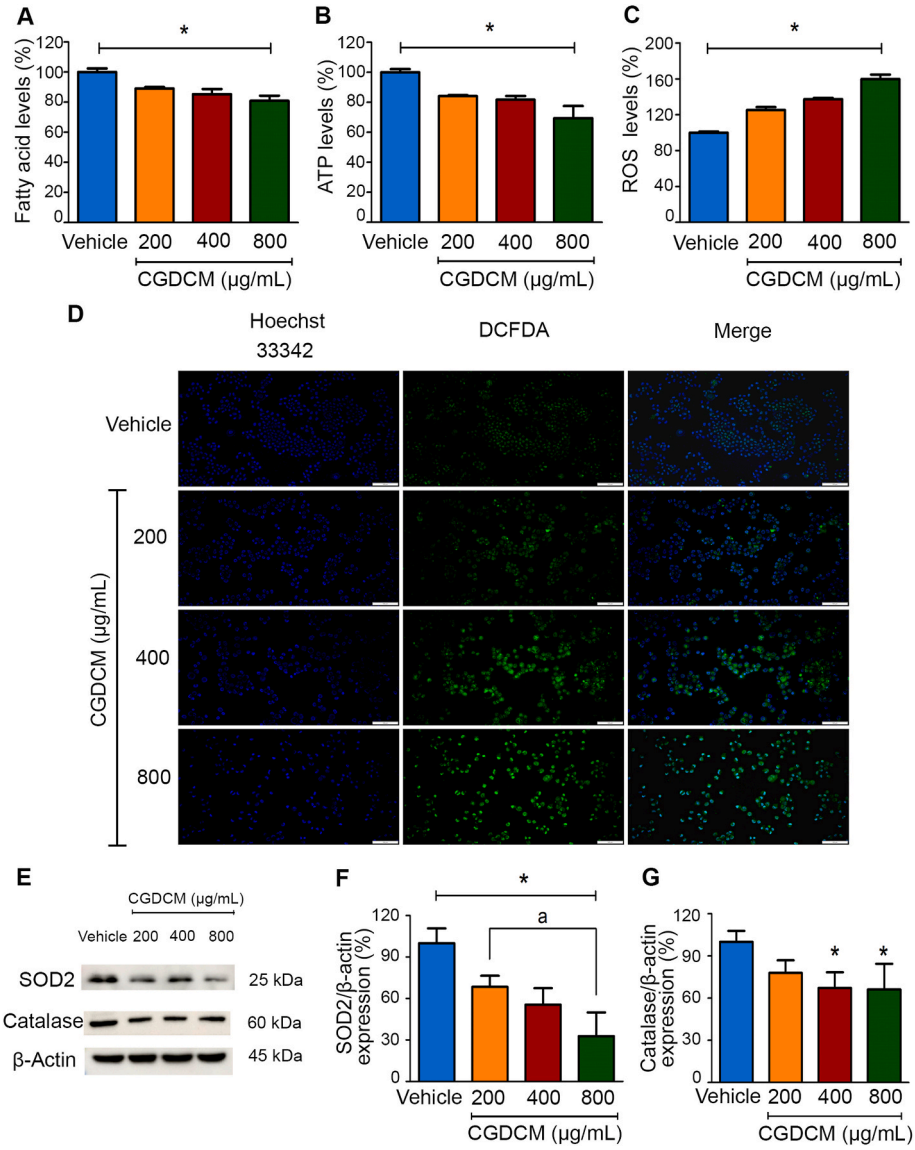

Fig. 4. The effect of CGDCM on the percentage of (A) fatty acids, (B) ATP, and (C) ROS levels in HepG2 cells. Cells were treated for 24 h with 200, 400, and 800 μg/mL CGDCM and 0.8% DMSO as the vehicle control. (D) ROS were analyzed by fluorescence staining with H2DCFDA and then observed with a fluorescence microscope, Bars = 100 μm. (E) SOD2 and catalase expression determined by western blotting. (F) The relative expression levels of SOD2/β-actin and (G) catalase/β-actin. The original uncropped western blots of SOD2, catalase, and β-actin are presented in the Supplementary Fig. S2. Data are presented as the mean ± SD from at least three replicates, n = 3, and statistics were analyzed with one-way ANOVA with Tukey's HSD test. *$p < 0.05$ vs. the vehicle.

3.5. *ROS production induced by CGDCM played a major role in apoptosis and MMP disruption*

Following NAC pretreatment for 2 h, ROS were significantly reduced after CGDCM treatment in HepG2 cells compared to non-NAC treatment (Fig. 5A and B). The restoration of MMP to normal levels in cells treated with CGDCM and NAC verified the importance of ROS production in apoptosis upon CGDCM treatment (Fig. 5C and D). Therefore, these findings suggest that ROS production mediates CGDCM-induced mitochondrial-dependent apoptosis in HepG2 cells.

3.6. *The property of the C. gigantea extracts on CYPs450 activities*

To study the potential inhibitory action of four extract fractions, CGEtOH, CGDCM, CGEtOAc, and CGW on various CYP isoforms present in human liver microsomes, CYP1A2-dependent ethoxyresorufin-*O*-de-ethylation, CYP2C9-dependent tolbutamide hydroxylation, CYP2E1-dependent *p*-nitrophenol hydroxylation, and CYP3A4-dependent 6β-testosterone hydroxylation were tested. As

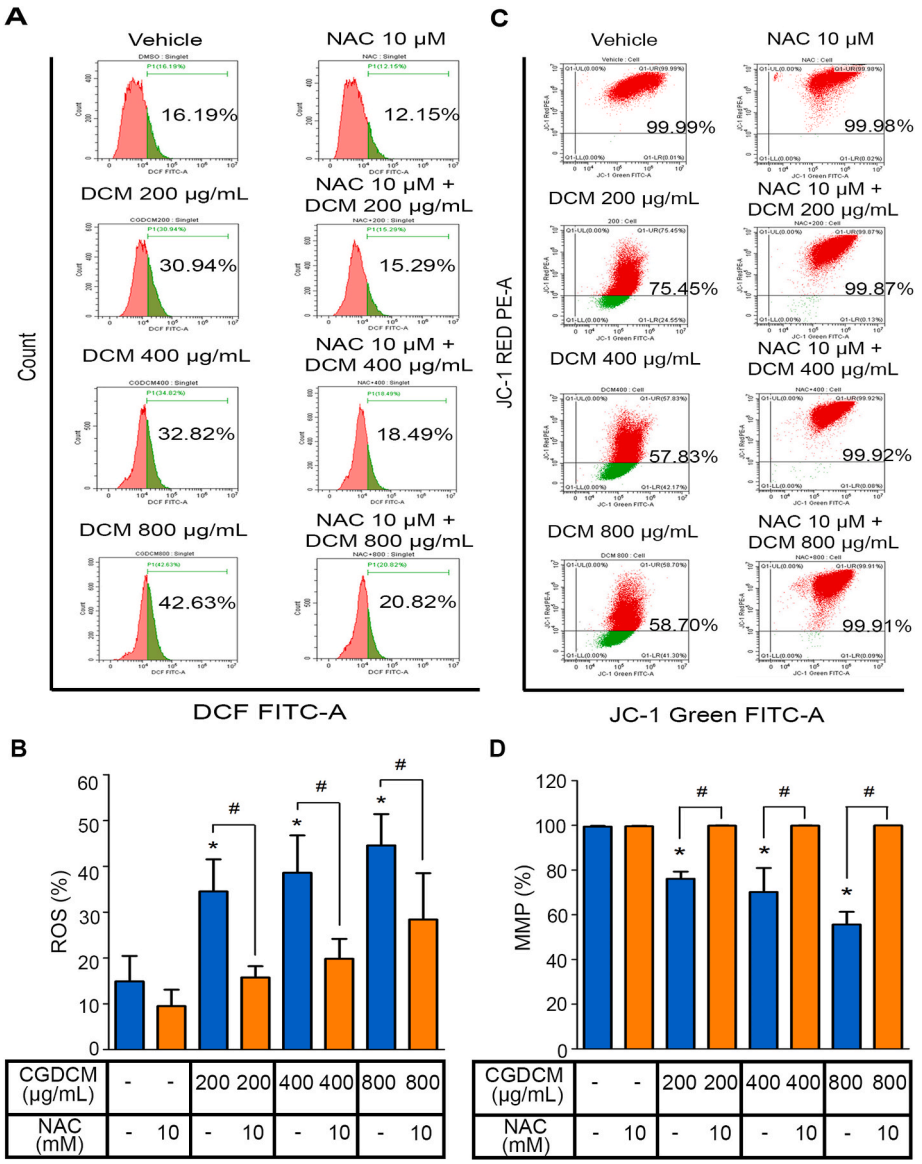

Fig. 5. Effects of CGDCM on ROS production and dissipation of MMP in HepG2 cells pretreated with *N*-acetylcysteine (NAC) for 2 h. Cells were treated for 24 h with 200, 400, and 800 μg/mL CGDCM and 0.8% DMSO as the vehicle control. (A) A representative flow cytometric image of ROS generation. (B) The percentage of ROS production. (C) A representative MMP was detected using flow cytometric staining of cells with JC-1. (D) The percentage of dissipation of MMP. Data are presented as the mean ± SD from at least three replicates, n = 3, and statistics were analyzed with one-way ANOVA with Tukey's HSD test. *p < 0.05 vs. the vehicle.

Table 2
The inhibitory effects (IC50 (μg/mL)) of the *C. gigantea* extracts and standard drugs on CYP-specific model activities.

Sample	Inhibitory effects to CYP isoforms (IC50) (μg/mL)			
	CYP1A2	CYP2C9	CYP2E1	CYP3A4
CGEtOH	>1000	12.11	>1000	101.2
CGDCM	>1000	59.56	>1000	56.54
CGEtOAc	>1000	20.43	>1000	81.52
CGW	>1000	46.38	>1000	296.9
α-naphthoflavone	0.34	–	–	–
Sulfaphenazole	–	0.45	–	–
Disulfiram	–	–	0.25	–
Ketoconazole	–	–	–	2.59

shown in Table 2, the results indicated that all four fractions were weak inhibitors of CYP1A2 and CYP2E1 isoforms (IC50 > 1000 μg/mL). The inhibitory effects of these four fractions on CYP3A4 were moderate (IC50 = 56.54–296.9 μg/mL). CGDCM and CGW exhibited moderate inhibitory effects on CYP2C9 in human microsomes (IC50 = 59.56 and 46.38 μg/mL, respectively). Interestingly, the effects of CGEtOH and CGEtOAc on CYP2C9 were quite strong inhibition activities (IC50 = 12.11 and 20.43 μg/ml, respectively). The information obtained from *C. gigantea* extracts provides the cause of drug-herb interactions in humans, especially through lower CYP2C9 activity, which would assist in the further development of bioactive compounds found in *C. gigantea* extracts to improve the bioavailability of oral or local dosage forms together with avoiding drug-herb interactions once used with other medications.

4. Discussion

The total amounts of phytochemicals, i.e., cardiac glycosides, triterpenoids, and phenolic compounds, in the four fractions were quite similar to our reported values [10,22]. The calotropin and calactin contents among the four fractions showed the same trends as our previous reports [10,22]. However, a slightly lower content of calotropin and a higher content of calactin compared to previously reported values were found. This might be due to several factors, such as different lots of plant materials and some differences in the extraction protocol. The different types and levels of phytochemicals in the studied fractions may influence the effectiveness of the extracts in inhibiting the proliferation of cancer cells. CGDCM and CGEtOAc, which contain higher concentrations of secondary metabolites such as calactin, calotropin, triterpenoids, cardiac glycosides, and phenolic compounds, demonstrate greater cytotoxic activity against various cancer cell lines than CGEtOH and CGW, which contain lower concentrations of secondary metabolites [11, 23].

It has been hypothesized that the anticancer properties of the stem bark extract from *C. gigantea* correlate with its active ingredients, with the dichloromethane fraction containing the highest levels of triterpenoids, followed by cardiac glycoside, flavonoid, alkaloid, phenolic, and calotropin concentrations [10]. Additionally, calotropin from *C. gigantea* was discovered to have a cytotoxic effect on cancers [32]. *C. gigantea* latex and fruit calotropin compound suppressed transcriptional HIF-1 activity in human breast cancer cells [23]. Calotropone and gofruside isolated from the ethanolic extract fraction of *C. gigantea* roots reduced the viability of cancer cells [33]. Rutinosides and isorhamnetin-3-*O*-rutinoside, two prevalent flavonoids in the entire plant extract of *C. gigantea*, induced apoptosis in non-small cell lung cancer A549 and NCL-H1299 cells [7].

The formation of ROS is considered to be one of the primary mechanisms underlying the anticancer properties of the extracts of *C. gigantea* as well as other plant-derived compounds [2,10,12–14]. Numerous pathways have been identified for the effect of *C. gigantea* extracts to trigger ROS production in cancer cells. The elevated ROS levels that mediated apoptosis in lung cancer A549 and NCI–H1299 cells after incubation with *C. gigantea* whole plant extracts resulted from a reduction in the expression of the ROS scavengers superoxide dismutase and catalase [7]. Similarly, suppression of antioxidant molecule expression in lung carcinoma A459 cells caused an elevation of ROS production after treatment with the cardenolide coroglaucigenin found in the stem and leaf extracts of *C. gigantea* [11]. Increased ROS accumulation induced apoptosis in cancer cells by increasing the mitochondrial permeability transition pore to cause mitochondrial damage, as observed in hepatocellular carcinoma (SMMC-7721) cells treated with α-hederin, a secondary saponin derived from *Hedera* or *Nigella species* [34]. ROS-induced apoptosis in gastric cancer cells was found to be regulated by suppression of the Stat3/JAK2 signaling pathway following treatment with leaves and seed coat anacardic acid, ginkogolic acid, extracted from *Ginkgo biloba* L [31].

This study reveals that a decrease in fatty acids in HepG2 cells by the CGDCM fraction from *C. gigantea* stem bark extract influences apoptotic induction. There was, however, no evidence demonstrating the mechanism by which CGDCM inhibits fatty acid production. Several studies have demonstrated the effect of plant extracts on the signaling pathways that regulate the synthesis of fatty acids in cancer cells. A diterpene, kahweol, found in *Arabica* coffee beans, causes apoptosis by inhibiting fatty acid synthesis through the PI3K/Akt/mTOR/SREBP signaling pathway reported in HER2-overexpressing cancer cells [15]. α-Mangostin extracted from *Garcinia mangostana* L. inhibited cell proliferation and induced apoptosis by suppressing the expression of key enzymes in the de novo lipogenesis pathway via activation of AMPK/SREBP1 signaling in gallbladder cancer cells [16].

The association between the anticancer effects of plant extracts and ATP generation has been reported. Reduced ATP levels were observed to activate apoptosis following treatment of lung cancer cells with the flavanonol glycoside engeletin (dihydrokaempferol 3-rhamnoside) found in the skin of white grapes and white wine [18], *C. gigantea* stem bark extract-treated colon cancer cells [10], and curcumin from the Zingiberaceae *Curcuma longa*-treated murine lymphocytic leukemia: L1210, murine breast: 4T1, murine melanoma: B16, and murine colon: CT26 cancer cells [12]. It was reported that a decrease in ATP levels contributes to an increase in ROS levels, which enhances apoptosis in cancer cells. The effect of α-hederin, a secondary saponin found in *Hedera* or *Nigella species*, demonstrated that decreased ATP levels result in increased amounts of ROS, which in turn reduces the potential of the mitochondrial membrane and promotes death [34], similar to the effect of curcumin, which revealed a decrease in ATP biosynthesis that stimulated ROS production and caused endoplasmic reticulum stress in cancer cells [12].

The *C. gigantea* extracts may show their ability to lower CYP2C9 activity, which may cause drug-herb interactions. However, when comparing the IC50 of the extracts to standard inhibitors of each type of CYP (CYP1A2, CYP2C9, CYP2E1 and CYP3A4), the IC50 values of α-naphthoflavone, sulfaphenazole, disulfiram and ketoconazole were 0.34, 0.45, 0.25 and 2.59 μg/ml, respectively, as shown in Table 2. The IC50 values of the four extracts were more than 25 times higher than those of all four CYPs. This indicated that the *C. gigantea* stem bark extracts might be less likely to induce drug-herb interactions through these CYPs450.

This study revealed that the cytotoxic effect of *C. gigantea* extract was equal to that of sorafenib after 24 h of treatment in HepG2 cells, with an IC50 of approximately 8 μM. According to numerous studies, the IC50 values after 24 and 48 h of sorafenib exposure were 19.5 ± 1.4 and 12.0 ± 3.1 μM [35], and after 72 h, it was 7.42 μM [36] in HepG2 cells.

This research has some potential limitations, including that it may need to investigate the effects of *C. gigantea* extracts on an additional variety of cancer cells. In order to apply *C. gigantea* extracts in the future as potentially effective alternative anticancer agents, their efficacy should be evaluated in cancer models, particularly those with resistance to chemotherapeutic drugs. In addition, there may be advantages to studying the effects of CGDCM at high concentrations on animal models as part of ongoing research. However, quantitative analysis of additional groups of secondary metabolites, such as triterpenoids or phenolic compounds, may be good options for selecting some compounds to be used as bioactive markers in the future. In addition, mass spectrometry may be a more sensitive technique for the further development of quality control protocols for the potent extracts.

5. Conclusions

C. gigantea stem bark extracts produced a potent anticancer effect in HepG2 cells and inhibitory effects on CYP450 activities, which will provide knowledge assets for future research to improve anticancer efficacy employing various plant-based extract regimens and to avoid drug-herb interactions in the future.

Data availability statement

Data included in article/supplementary material/referenced in article.

Author contribution statement

P.Su.: handled most of the experiment, received the funding acquisition, provided the methodology and software for validation, analyzed the formal analysis, drafted the original manuscript, reviewed, edited and approved the final manuscript. A.W.: received the funding acquisition, reviewed, edited and approved the final manuscript. O.S.: edited and approved the final manuscript. J.S.: edited and approved the final manuscript. S.P.: designed the conceptualization, analyzed the data management, received the funding acquisition, handled most of the experiment, provided the methodology and software for validation, analyzed the formal analysis, drafted the original manuscript, reviewed, edited and approved the final manuscript. D.P.: designed the conceptualization, analyzed the data management, handled most of the experiment, provided the methodology and software for validation, analyzed the formal analysis, drafted the original manuscript, reviewed, edited and approved the final manuscript. P.Sr.: designed the conceptualization, analyzed the data management, received the funding acquisition, handled most of the experiment, provided the methodology and software for validation, analyzed the formal analysis, drafted the original manuscript, reviewed, edited and approved the final manuscript

Funding

The funding for this study is from the National Science, Research and Innovation Fund of Thailand (NSRF) [Grant No. R2564B033 to A.W.], the National Science, Research and Innovation Fund of Thailand (NSRF) [Grant No. R2564B007 to S.P. and P.Sr.], the Agricultural Research Development Agency (Public Organization) [Grant NO. CRP6505030030 to S.P.], and the graduate thesis funding from Faculty of Medical Science, Naresuan University, Phitsanulok, Thailand [Grant No. 62063546 to P.Su.]. The funders play no role in study design, data collection and analysis, publication decisions, or manuscript preparation.

Declaration of competing interest

All authors have no competing financial interests or personal relationships that influence this study.

Appendix A. Supplementary data

Supplementary data related to this article can be found at https://doi.org/10.1016/j.heliyon.2023.e16375.

References

[1] R.L. Siegel, K.D. Miller, A. Jemal, Cancer statistics, Ca-Cancer J. Clin. 70 (2020) 7–30.
[2] T. Hu, K. Linghu, S. Huang, M. Battino, M.I. Georgiev, G. Zengin, D. Li, Y. Deng, Y.T. Wang, H. Cao, Flaxseed extract induces apoptosis in human breast cancer MCF-7 cells, Food Chem. Toxicol. 127 (2019) 188–196.
[3] S.U.F. Syed Najmuddin, M.F. Romli, M. Hamid, N.B. Alitheen, N.M.A. Nik Abd Rahman, Anti-cancer effect of Annona Muricata Linn leaves crude extract (AMCE) on breast cancer cell line, BMC Complementary Altern. Med. 16 (2016) 311.
[4] T. Kanchan, A. Atreya, Calotropis gigantea, Wilderness Environ. Med. 27 (2016) 350–351.
[5] M.R. Habib, M.R. Karim, Effect of anhydrosophoradiol-3-acetate of *Calotropis gigantea* (Linn.) flower as antitumoric agent against Ehrlich's ascites carcinoma in mice, Pharmacol. Rep. 65 (2013) 761–767.
[6] R. Mutiah, Sukardiman, A. Widyawaruyanti, Cytotoxic effect of crude extract and fraction from *Calotropis gigantea* leaves on human colon cancer WIDR cell lines, Int. J. Pharm. Pharm. Sci. 9 (2016) 83.

[7] J. Lee, H.-J. Jang, H. Chun, T.-H. Pham, Y. Bak, J.-W. Shin, H. Jin, Y.-I. Kim, H.W. Ryu, S.R. Oh, D.-Y. Yoon, *Calotropis gigantea* extract induces apoptosis through extrinsic/intrinsic pathways and reactive oxygen species generation in A549 and NCI-H1299 non-small cell lung cancer cells, BMC Complementary Altern. Med. 19 (2019) 134.
[8] R. Mutiah, S. Sukardiman, A. Widyawaruyanti, S. Zulaikah, Comparison of ethanol extract from roots, leaves, and flowers of *Calotropis gigantea* as anticancer on T47D breast cancer cell lines, ALCHEMY 5 (2018) 1.
[9] K.R. Kharat, A.S. Kharat, The *Calotropis gigantea* methanolic extract induces apoptosis in human breast carcinoma cells, Iran. J. Med. Sci. 44 (2019) 483–492.
[10] T. Winitchaikul, S. Sawong, D. Surangkul, M. Srikummool, J. Somran, D. Pekthong, K. Kamonlakorn, P. Nangngam, S. Parhira, P. Srisawang, *Calotropis gigantea* stem bark extract induced apoptosis related to ROS and ATP production in colon cancer cells, PLoS One 16 (2021), e0254392.
[11] M. Sun, D. Pan, Y. Chen, Y. Li, K. Gao, B. Hu, Coroglaucigenin enhances the radiosensitivity of human lung cancer cells through Nrf2/ROS pathway, Oncotarget 8 (2017) 32807–32820.
[12] G. Bianchi, S. Ravera, C. Traverso, A. Amaro, F. Piaggio, L. Emionite, T. Bachetti, U. Pfeffer, L. Raffaghello, Curcumin induces a fatal energetic impairment in tumor cells in vitro and in vivo by inhibiting ATP-synthase activity, Carcinogenesis 39 (2018) 1141–1150.
[13] Cha Park, Lee Choi, Hwang-Bo, Kim Ji, Hong Kim, Kim Cheong, Hwang Yun, Choi Kim, Isorhamnetin induces cell cycle arrest and apoptosis via reactive oxygen species-mediated AMP-activated protein kinase signaling pathway activation in human bladder cancer cells, Cancers 11 (2019) 1494.
[14] S. Sur, H. Nakanishi, C. Flaveny, J.E. Ippolito, J. McHowat, D.A. Ford, R.B. Ray, Inhibition of the key metabolic pathways, glycolysis and lipogenesis, of oral cancer by bitter melon extract, Cell Commun. Signal. 17 (2019) 131.
[15] S.H. Oh, Y.P. Hwang, J.H. Choi, S.W. Jin, G.H. Lee, E.H. Han, Y.H. Chung, Y.C. Chung, H.G. Jeong, Kahweol inhibits proliferation and induces apoptosis by suppressing fatty acid synthase in HER2-overexpressing cancer cells, Food Chem. Toxicol. 121 (2018) 326–335.
[16] Y. Shi, Y. Fan, Y. Hu, J. Jing, C. Wang, Y. Wu, Q. Geng, X. Dong, E. Li, D. Dong, α-Mangostin suppresses the de novo lipogenesis and enhances the chemotherapeutic response to gemcitabine in gallbladder carcinoma cells via targeting the AMPK/SREBP1 cascades, J. Cell Mol. Med. 24 (2020) 760–771.
[17] K.B. Singh, S.-H. Kim, E.-R. Hahm, S.K. Pore, B.L. Jacobs, S. v Singh, Prostate cancer chemoprevention by sulforaphane in a preclinical mouse model is associated with inhibition of fatty acid metabolism, Carcinogenesis 39 (2018) 826–837.
[18] T. Liu, Y. Li, J. Sun, G. Tian, Z. Shi, Engeletin suppresses lung cancer progression by inducing apoptotic cell death through modulating the XIAP signaling pathway: a molecular mechanism involving ER stress, Biomed. Pharmacother. 128 (2020), 110221.
[19] S.A. Baba, S.A. Malik, Determination of total phenolic and flavonoid content, antimicrobial and antioxidant activity of a root extract of *Arisaema jacquemontii* Blume, J. Taibah Univ. Sci. 9 (2015) 449–454.
[20] C.L. Chang, C.S. Lin, G.H. Lai, Phytochemical Characteristics, free Radical scavenging activities, and Neuroprotection of five Medicinal plant extracts, Evid. base Compl. Alternative Med. 2012 (2012) 1–8.
[21] Z. Tofighi, S.N. Ghazi, A. Hadjiakhoondi, N. Yassa, Determination of cardiac glycosides and total phenols in different generations of Securigera securidaca suspension culture, Res. J. Pharmacogn. 3 (2016) 25–31.
[22] S. Sawong, D. Pekthong, P. Suknoppakit, T. Winitchaikul, W. Kaewkong, J. Somran, C. Intapa, S. Parhira, P. Srisawang, *Calotropis gigantea* stem bark extracts inhibit liver cancer induced by diethylnitrosamine, Sci. Rep. 12 (2022), 12151.
[23] S. Parhira, G.-Y. Zhu, M. Chen, L.-P. Bai, Z.-H. Jiang, Cardenolides from *Calotropis gigantea* as potent inhibitors of hypoxia-inducible factor-1 transcriptional activity, J. Ethnopharmacol. 194 (2016) 930–936.
[24] P. Parsonidis, I. Vlachou, A. Mamagkaki, I. Bouris, V. Daikopoulou, I. Papasotiriou, Evaluation of Tegaran Formula ZhenHua cytotoxicity against human cancer cell lines, PLoS One 15 (2020), e0240969.
[25] M.D. Burke, S. Thompson, C.R. Elcombe, J. Halpert, T. Haaparanta, R.T. Mayer, Ethoxy-, pentoxy- and benzyloxyphenoxazones and homologues: a series of substrates to distinguish between different induced cytochromes P-450, Biochem. Pharmacol. 34 (1985) 3337–3345.
[26] M.v. Relling, T. Aoyama, F.J. Gonzalez, U.A. Meyer, Tolbutamide and mephenytoin hydroxylation by human cytochrome P450s in the CYP2C subfamily, J. Pharmacol. Exp. Ther. 252 (1990) 442–447.
[27] J.W. Allis, B.L. Robinson, A kinetic assay for p-nitrophenol hydroxylase in rat liver microsomes, Anal. Biochem. 219 (1994) 49–52.
[28] R.E. Pearce, C.J. McIntyre, A. Madan, U. Sanzgiri, A.J. Draper, P.L. Bullock, D.C. Cook, L.A. Burton, J. Latham, C. Nevins, A. Parkinson, Effects of freezing, thawing, and storing human liver microsomes on cytochrome P450 activity, Arch. Biochem. Biophys. 331 (1996) 145–169.
[29] P. Khiewkamrop, P. Phunsomboon, L. Richert, D. Pekthong, P. Srisawang, Epistructured catechins, EGCG and EC facilitate apoptosis induction through targeting de novo lipogenesis pathway in HepG2 cells, Cancer Cell Int. 18 (2018) 46.
[30] P. Khiewkamrop, D. Surangkul, M. Srikummool, L. Richert, D. Pekthong, S. Parhira, J. Somran, P. Srisawang, Epigallocatechin gallate triggers apoptosis by suppressing *de novo* lipogenesis in colorectal carcinoma cells, FEBS Open Bio 12 (2022) 937–958.
[31] J.-R. Liang, H. Yang, Ginkgolic acid (GA) suppresses gastric cancer growth by inducing apoptosis and suppressing STAT3/JAK2 signaling regulated by ROS, Biomed. Pharmacother. 125 (2020), 109585.
[32] L. Zhou, L. Cai, Y. Guo, H. Zhang, P. Wang, G. Yi, Y. Huang, Calotropin activates YAP through downregulation of LATS1 in colorectal cancer cells</p&gt, OncoTargets Ther. 12 (2019) 4047–4054.
[33] Z.-N. Wang, M.-Y. Wang, W.-L. Mei, Z. Han, H.-F. Dai, A New cytotoxic Pregnanone from *Calotropis gigantea*, Molecules 13 (2008) 3033–3039.
[34] J. Li, D.-D. Wu, J.-X. Zhang, J. Wang, J.-J. Ma, X. Hu, W.-G. Dong, Mitochondrial pathway mediated by reactive oxygen species involvement in α-hederin-induced apoptosis in hepatocellular carcinoma cells, World J. Gastroenterol. 24 (2018) 1901–1910.
[35] M. Cervello, D. Bachvarov, N. Lampiasi, A. Cusimano, A. Azzolina, J.A. McCubrey, G. Montalto, Molecular mechanisms of sorafenib action in liver cancer cells, Cell Cycle 11 (2012) 2843–2855.
[36] J. Liu, Y. Liu, L. Meng, B. Ji, D. Yang, Synergistic Antitumor effect of sorafenib in Combination with ATM inhibitor in hepatocellular carcinoma cells, Int. J. Med. Sci. 14 (2017) 523–529.